Heliyon 10 (2024) e26068

Contents lists available at ScienceDirect

Heliyon

journal homepage: www.cell.com/heliyon

Research article

Directional fracturing of rock by soundless chemical demolition agents

Ivan Sakhno *, Svitlana Sakhno

Donetsk National Technical University, 29, Sofia Kovalevska Street, Lutsk, Volyn region, 43012, Ukraine

ARTICLE INFO

Keywords:
Rock fracturing
Rock blasting
Rock excavation
Tensile stress
Mining
Rock mechanics
Stress concentration cartridge

ABSTRACT

Rock fracturing is one of the main processes in the modern mining, mineral recovery, and energy industry, which is associated with the numerous environmentally harmful influences. Environmentally friendly alternative to conventional fracturing methods is non-explosive technology, which based on using of soundless chemical demolition agents (SCDA). In this study, method of directional fracturing, which based on creating tensile stress concentrators on the hole surface in the required location, was proposed. Considering the influences of additional installation in the borehole of stress concentration cartridge on stress field nearby the hole, a case study of the effectiveness of proposed rock fracturing method was performed in this paper. A numerical simulation was used to study the stress distribution around the borehole with SCDA in different rock types. It was found that cartridge installation leads to the occurrence of the tensile stress concentrations only near to the gap of the cartridge. The value of tensile stress concentration in the proposed rock fracturing method significantly depends on a cartridge gap distance. An increase in the gap distance leads to a decrease in the stress concentration factor. For granite, sandstone and mudstone, relationships of stress concentration factor to cartridge gap distance that was divided on hole diameter were obtained. The equation for calculating of the hole spacing for the directional fracturing method was proposed. The results of the study are confirmed by experiments in-situ on the directional fracturing of rocks in a quarry and in a coal mine.

1. Introduction

The most widely employed method of the rock-breaking is explosive one. Blasting has been regarded as the main effective and the most economically viable technique for rock excavation and fragmentation in open pit and underground mines. However, blasting is associated with the numerous environmentally harmful influences as ground vibration, generation of dust, air blast, fly rock and back-break [1–4]. Therefore, development and application of more environmentally friendly alternative to conventional methods of rock fracturing is an actual issue. Among the environmentally friendly approaches of rock fracturing is the electric method. The electric fragmentation is the one of the methods with minimal environmental impact. The electrical disintegration of rocks is generally used to the liberation of minerals containing metals of platinum group, refractory gold and silver, iron, copper, magnesium ilmenite, and of metals of smelter slags [5].

Seyed et al. [6] found that the specific liberation effect at the disintegration of phosphate ore by electrical pulses is due to the locality of the electrical field at the interface of mineral components of the phosphate ore aggregates with different permittivities. Li

* Corresponding author.
E-mail address: ivan.sakhno@donntu.edu.ua (I. Sakhno).

https://doi.org/10.1016/j.heliyon.2024.e26068
Received 25 June 2023; Received in revised form 6 February 2024; Accepted 7 February 2024
Available online 13 February 2024

et al. [7] established a high-voltage electropulse breakdown damage model for granite. The electrical disintegration of granite is studied mainly in relation to the drilling process [8,9]. The electrical fracturing of rock has limited application, mainly in the mineral liberation process, in which the generating current can be controlled. This method is environmentally friendly and receiving the attention of researchers, however, its application for directional fracturing has not been proposed.

Nowadays significant progress in the directional destruction of rocks has been made by the hydraulic fracturing method. Serdyukov [10] used a special fracturing device to generate tension in the rock along the axis of the hole. A fracture across a hole is created by means of additional shearing stress applied to the hole walls within the interval of the fracture. Deng et al. [11] investigated the influences of notch angle, notch length and injection rate on the directional hydraulic fracturing by a 3D nonlinear finite element method. Lu and He [12] studied linear collaborative directional hydraulic fracturing controlled by a pre-slotted guide and fracturing boreholes. Cheng et al. [13] proposed a novel method of directional hydraulic fracturing based on hydraulic slotting in a nonuniform pressure field.

The main negative ecological impact of hydraulic fracturing is the consumption of large volumes of fresh water [14]. Recent studies of Ellsworth [15] and Holland [16] claim that hydraulic injection induces seismic activation. The possible harmful effect on human health caused by toxic chemicals that are used in hydraulic fracturing is another negative aspect [17,18].

Another environmentally friendly alternative is the non-explosive expansion materials, also called soundless chemical demolition agents (SCDAs), which are widely applied as demolition of rock or concrete structures [19,20], mine excavation [21–23], and unconventional gas exploration [24]. SCDA is a powdery substance which tends to volumetric expands in hydration through the formation of calcium hydroxide or ettringite [25]. The SCDA hydration rate and the measured expansive pressure are affected by the diameter of the hole, water content, ambient temperature and rock properties and can exceed 50–80 MPa. The main characteristics of SCDA that determine the effectiveness of its use in mining are expansive pressure, fracturing time, stability to different temperature and water content. In these areas, the main efforts of scientists have been made. The SCDA expansion is caused by the hydration of CaO [26–28]. Therefore, the expansive pressure of SCDA is directly proportional to the CaO content in the mixture. However, attempts to increase the value of expansive pressure and its generation rate by increasing the proportion of CaO were ineffective. The consequence of increasing the proportion of CaO in the mixture is an uncontrollable increase in temperature, boiling off chemically unbound water from the mixture, and blowout of SCDA from the borehole [28,29].

Many studies have shown that water/SCDA ratio is inversely proportional to the value and rate of SCDA expansive pressure generating, while higher ambient temperatures and SCDA mixture result to earlier grow of expansive pressures [30–32]. However, controlling the expansive pressure generating rate and its value by heating of water (befor mixing) or SCDA mixture is not effective, because it leads to an uncontrollable increase in heat, and blowout of SCDA from the borehole. The reason of this phenomenon is the exothermic type of hydration reaction of CaO.

Now evident that, in order to enhance the rate of expansive pressure generation without the blowout of SCDA from the hole, adjustments must be made to SCDA systems, which are made by blending with other cementing compounds [19]. Numerous additives such as alkali hydroxides, silicates, fluorosilicates, and organic compounds were proposed as accelerators, which have different effects on hydration process of binders [33–36]. Dessouki et al. [33], proposed to accelerate SCDA volumetric expansion rate by adding of 15% $CaSO_4$. De Silva et al. [37] proposed to add a viscosity enhancing admixture (VEA) to improve the washout resistance of modified SCDA, which can effectively be used in underwater conditions. Maneenoi et al. [38] showed that adding 4 wt% $MgCl_2$ and 3 wt% $CaCl_2$ have accelerated the fracture onset by 47.4% and 61.2%, respectively. As reported in the mentioned studies, significant positive results have been obtained in the areas of studying and modifying of the SCDA properties. However, the fracturing mechanism and optimal parameters of fracturing still require further study to improve the effectiveness of SCDA. Nowadays, the control of the directional fracturing with the SCDA is carried out mainly by setting the direction of a row of holes. A desired propagation of the fracture network could be achieved by altering the size and spacing of boreholes and their arrangements [39,40].

Fracture control efforts have also focused on hole pattern optimization. For example Harada et al. [41] recommended a hexagonal borehole pattern to optimize the fracture density of rock. Such optimization usually consists in achieving of maximum destruction by a minimum number of holes. Gambatese [42] proposed to control the direction of fracturing by introducing non-injected SCDA boreholes in the rock. According to his experimental research, crack migration towards non-injected boreholes is around 35% in a grid of 6 $\times$ 6 boreholes. Guo et al. [43] studied the fracturing of rock by SCDA and analyzed the growth of fracture network in rock specimens. It was found that the surface fracture density in the experiment decreased with rock hardness growth. Depending on the orientation of rock discontinuities, complex fracture patterns were observed.

Conventionally SCDAs have been used in the demolition of concrete structures, and parts of buildings in urban settings [44–47]. Less commonly, SCDA was used in mining, for hard rock breakage or tunneling. Recently, researchers reported positive experiences of granite destruction in Saudi Arabia [48], granite extraction in India [49], and gneiss destruction in central Cameroon [50]. Non-conventionally the use of SCDA is associated with well cementing, as well as stimulating and enhancing fracturing for the oil and gas industry [51,52].

The directional fracturing by SCDA in mining is not studied. At the same time devices and techniques that were used for directional fracturing by other non-explosive methods can not be used with SCDA. In this study, the term “directional fracturing” means the controlled creation of a main crack in the desired direction while excluding the occurrence of other cracks.

The key to applicability of SCDA in rock directional fragmentation is to control the fracture initiation, and propagation. Unlike other fracturing methods, which form multiple radial cracks, SCDAs typically create three or rarely four cracks around the hole. However, SCDA can produce one crack with the required orientation. A desired propagation of the fracture network is usually achieved by changing the size and spacing of boreholes and their arrangements [25]. During the SCDA hydration process, the equal pressure is created on the internal surface of the hole in all directions. In this case, the places of cracks initiation and their propagation are

determined by weaknesses of rocks and heterogeneity of them. Therefore, it is difficult to exclude undesirable fracturing along directions that do not coincide with the required ones. At the same time, the occurrence of additional cracks on the hole surface that do not coincide with the desired direction is possible.

In mining often becomes necessary to create a main crack of rocks. For example, in the case of main roof cutting in longwall mining with pillarless tecnology, extraction of precious and semiprecious stones with minimal crushing rate, etc. This study aims to explore the directional rock fracturing mechanism with SCDA and improving the method for calculating the borehole spacing. A non-explosive directional rock fragmentation technology was proposed in this study. The principle of directional rock fracturing was introduced. A numerical simulation of conventional SCDA fracturing and proposed rock fracturing methods was carried out. Then an experimental study on these methods was carried out for comparison. This paper proposed investigation of the effectiveness of directional rock fracturing by stress concentration cartridges. The optimal parameters for directional fracturing of rock were determined by numerical simulation method. The results of the study are confirmed by experiments in-situ in a granite quarry and in a coal mine.

2. Materials and methods

2.1. Principle of directional rock fracturing by SCDA

The conventional SCDA method is implemented in the following way. Powdery SCDA is mixed with water of appropriate quantity until a homogeneous slurry is obtained. After this SCDA slurry is poured into holes predrilled in rock. The distance between holes is calculated depending on the physical and mechanical properties of the SCDA and rocks. The diameter of the holes usually does not exceed 40 mm. The volumetric expansive pressure generates equal stress field in near-hole region in conventional SCDA method. In the near-contact region with the hole surface, the rock is under compression. However, as the SCDA expansion tends to increase the diameter of the hole, tensile stresses occur around it. When that tensile stress exceeds the tensile strength of the rocks, cracks will occur without the noise. These cracks are the result of tensile stresses that directed at right angles to the crack. Compressive stresses that aligned parallel to the crack do not have a significant effect on fracture, because the compressive strength of rocks is much higher than its tensile strength and the rate of stress transformation is low (Fig. 1a). In the case of single hole, the location of crack initiation is determined by the distance to the free surface, inhomogeneities of the rock, hidden cracks and defects. In the case of two holes or more, cracks initiate and propagate between them, when the distance between holes is calculated correctly and there are no defects in the rock.

The main fracturing parameters are the hole diameter and the borehole spacing. Most researchers and SCDA manufacturers recommend using borehole diameters in range from 30 mm to 60 mm. To calculate the hole spacing, empirical relations and equations are obtained on the basis of continuum mechanics.

Gomez and Mura [39] proposed an Equation (1) to find the borehole spacing (S) as follows:

$$S = k \times D \tag{1}$$

where D – the borehole diameter;

k – the empirical coefficient, given by Equation (2):

$$k = \frac{\pi}{\sqrt{8}} \left\{ \frac{4\vartheta_{SCDA}(1+\mu_{SCDA})\omega}{[\vartheta(1-2\mu)+\vartheta_{SCDA}]\sigma_c} \right\}^{1/2} \tag{2}$$

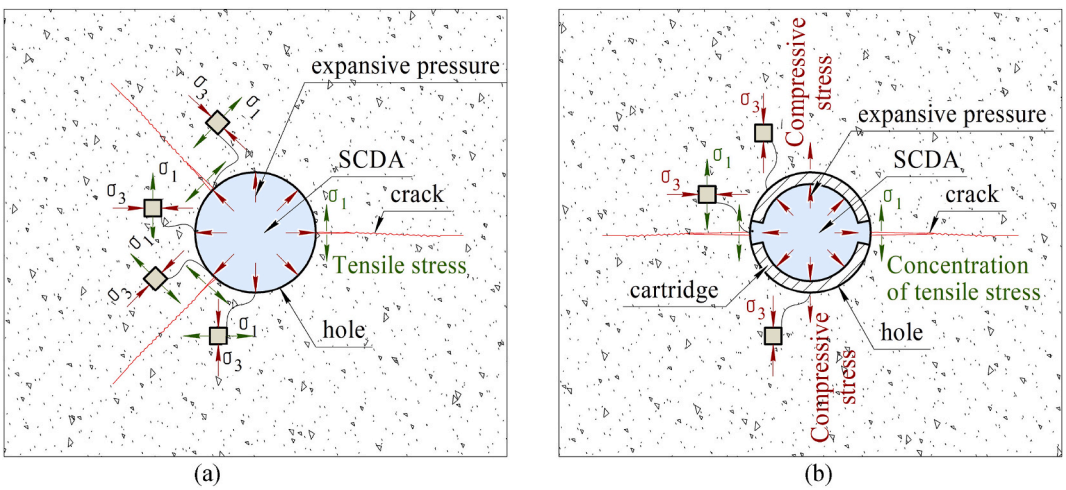

Fig. 1. Rock fracturing mechanism: (a) conventional SCDA method; (b) proposed SCDA method.

where $\mu_{SCDA}, \vartheta_{SCDA}$ – the Poisson's ratio and shear modulus of SCDA, respectively;

μ, ϑ – the Poisson's ratio and shear modulus of rock, respectively;
ω – the expansive strain of the SCDA;
σ_c – the fracture stress of the rock.

Jin et al. [40] proposed an Equation (3) to determine necessary hole spacing as follows:

$$S = 2D \times P\left(\frac{\sigma_c - \sigma_t}{\sigma_c \times \sigma_t}\right) \tag{3}$$

where P – the expansive pressure of SCDA;
σ_c, σ_t – compressive and tensile strengths of rock, respectively.
Arshadnejad [27] proposed Equation (4) to find the optimum borehole spacing:

$$S = \left[-0.285\left(\frac{P}{\sigma_t}\right)^2 + 3.5\left(\frac{P}{\sigma_t}\right) - 7.2\right] \frac{t^{2.7} E_r^{0.82} D^2}{K_{1C}^2} \tag{4}$$

where E_r – the elastic modulus of the rock;
$t-$ the hydration time;
K_{1C} – the stress intensity factor.In the study by Sakhno et al. [23], an equation for calculating the crack length (L_{cr}) was proposed, that is based on the Griffith energy criterion. This equation is also recommended to determine the hole spacing as follows:

$$L_{cr} = S = \frac{3P^2 \times \pi \times r_0^2 \times E_r}{8E_{SCDA} \times K_I^2}(1 - 2\mu_{SCDA}), \tag{5}$$

where.

r_0 – the hole radius;
E_{SCDA} – the elastic modulus of SCDA;
μ_{SCDA} – the Poisson's ratio of SCDA.

The idea underlying the proposed method of directional fracturing is to create tensile stress concentrators on the hole surface in the required location.

The implementation of this idea is carried out by additional installation of a stress concentration cartridge in the borehole. The SCDA is placed inside the cartridge as shown in Fig. 1b. The cartridge consists of two elements. Each element is a half of a steel pipe (AISI 1030 steel ASTM) with an outer diameter equal to the diameter of the borehole, obtained by longitudinal cutting. This steel was not specially selected; the result does not depend on the type of steel. The cartridge elements have closed ends, as shown in Fig. 2. Fig. 2a shows SCDA cartridge placed inside a borehole, that was drilled into a granite block. The design of the cartridge and its elements is shown in Fig. 2b.

In this case, expansive pressure of SCDA generates increased tensile stress in one of the hole diametral directions that coinciding with the gap of cartridge. At the same time in other directions, the cartridge protects against the occurrence of high tensile stress near

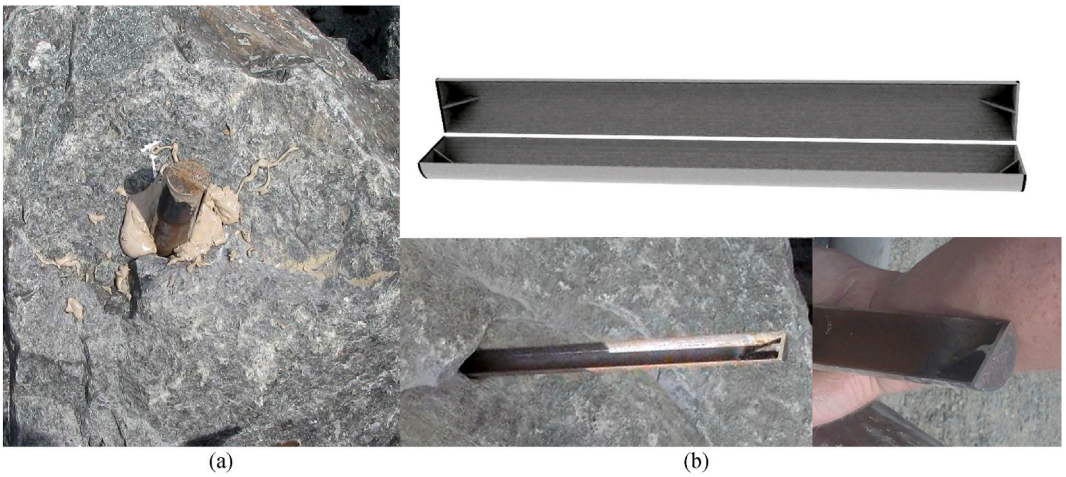

(a) (b)

Fig. 2. Stress concentration cartridge: (a) cartridge with SCDA in granite; (b) cartridge elements.

the surface of the hole. Tensile stress concentrations are sites of crack initiation in the rock. When that tensile stress exceeds the tensile strength of the rock, crack will occur in the required direction. Propagation of crack is provided by influence of tensile stress while the SCDA expands. In this way, directional rock fracturing is provided. For such fracturing, the borehole spacing calculation must be modified.

2.2. Experimental study of SCDA

In this study, SCDA from Ukraine (IDM slow series, vsv.ua.market) was used, which has an approximate component percentage by mass: soda ash - 2.3–7.0; sodium humate - 0.8–4.6; 20–40% aqueous solution of Sika BV 3 M – 30; quicklime is the residue. Thus water-agent ratio was 1:3. SCDA was a thick mixture that did not infiltrate to the rock. Flow table test of SCDA was 54 cm. In the process of hydration, SCDA hardens. The increase in expansion pressure occurs in the solid phase. Therefore the mixture is not coming out from borehole. Volumetric expansion of SCDAs is mainly caused by the exothermic reaction of calcium oxide under hydration as given by Equation (6) [27,28]:

$$CaO + H_2O \rightarrow Ca(OH)_2 + 15.2 \uparrow (\text{kCal / mol}) \quad (6)$$

The expansive pressure is generated in SCDA as a result of переводанглийскийрусскийlimitation given by the surrounding solid, so the value of its pressure depends on the strain of surrounding material. The current methods for determination of SCDA expansion pressure (expansive tube method, strain gauge method) are usually based on measurements at very small strains (1-2 $\times$ 10^{-3}), which does not correspond to the actual mechanism of expansion in the hole. By the current methods the maximum expansion pressure is determined in the strain conditions close to null. However, this pressure is not a constant, it depends on the actual increase of the SCDA volume. It is known that in a free state (with zero external resistance), for example, in a thin rubber shell, the volume of SCDA during hydration increases by 2.5–3 times. Depending on the deformational properties of the rock, the walls of the hole under the action of the internal pressure of the SCDA can be displaced by a different amount. This leads to an increase of the SCDA volume, which is followed by decrease in the expansion pressure relative to the deformation mode at zero strain. It is quite difficult to measure the expansion pressure at different SCDA volume increments by the conventional methods. However, taking into account the dependence of the expansion pressure on the increase of SCDA strain will make it possible more correctly calculate the parameters of rock fracture with different mechanical properties.

The special device was made to study the behavior of SCDA for various strains rate. The device consisted of a steel cylinder (AISI 1030 steel ASTM) with an internal diameter equal to the diameter of the borehole (40 mm) and a piston between which the SCDA was located (Fig. 3). The thickness of the cylinder wall was 20 mm, which guaranteed zero radial deformation. The device was installed between the plates of the press. Then the moving down of the piston was blocked by blocking nuts. They were installed between the piston and the cylinder. After that the initial pressure was created by the press. Blocking nuts prevent the compressing of SCDA by the initial pressure. At the initial stage of the experiment, SCDA retains the initial volume. As soon as the SCDA expansive pressure overcomes the initial pressure of the press and begins to increase in volume, this is fixed by the mechanical displacement indicator with a dial, as can be seen in Fig. 3. Further SCDA expansion leads to an increase in its pressure and vertical displacement. The expansive pressure increase is fixed by the press indicator. In this case, the volumetric expansion develops only vertically, which allows to fix pressure and strain in the corresponding strain mode. The initial pressure was varied during the experiments. The tests were carried out in five strain modes in which the initial pressure was 0 MPa (strain mode I), 10 MPa (strain mode II), 20 MPa (strain mode III), 40 MPa (strain mode IV), 50 MPa (strain mode V), respectively. The strains were changed from 0.002 (min strain mode, 50 MPa initial pressure) to 0.065 (max strain mode, 0 MPa initial pressure), which made it possible to obtain a relationship between the SCDA expansion pressure and the corresponding strains. Ambient temperature was 25 °C.

The evolutions of SCDA expansive pressure and strain over time for maximum and minimum stain modes are shown in Fig. 4a.

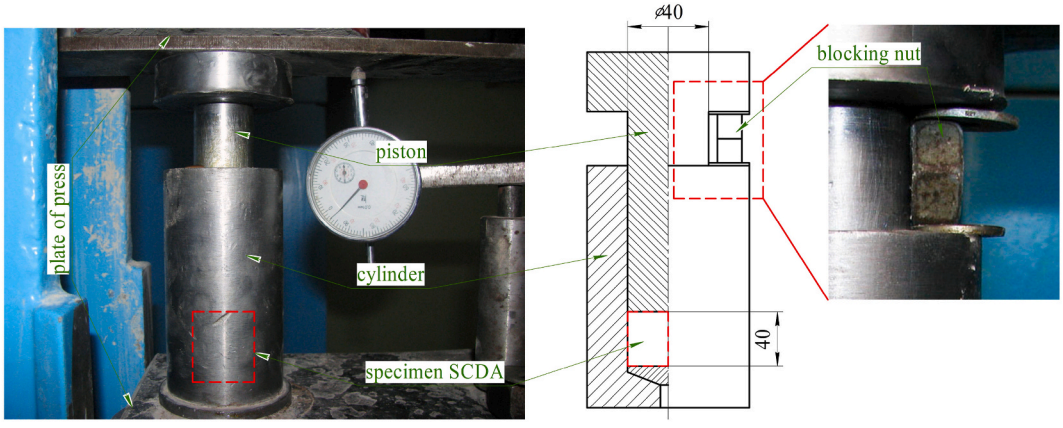

Fig. 3. The experimental setup for SCDA expansion ratio tests.

Relationships of SCDA expansive pressure to its strain for different strain modes are presented in Fig. 4b. Each curve in Fig. 4b shows the rise in expansive pressure and the corresponding strain over time for a specific strain mode. In this case, there is an inversely proportional relationship between strain and expansion pressure. The maximum expansive pressure of 50.6 MPa corresponds to 0.001 strain, and the minimum expansive pressure of 28.8 MPa corresponds to 0.065 strain.

According to Fig. 4a, the active chemical reaction of SCDA initiates in around 2 h. The maximum increase in expansive pressure is observed in the range of 2–8 h after mixing the components. The reaction rate gradually decreases and ends after 24 h. There is a directly proportional relationship between strain and expansive pressure, as shown in Fig. 4b. Reducing of the strains leads to an increase in the expansive pressure of SCDA in all strain modes. Based on the results of the laboratory tests, for the coefficient of reliability of approximation $R^2 = 0.93$, the dependence of expansive pressure P_{24} (after 24 h) on SCDA strain ε (in the strain range 0.001–0.065) is described by an exponential function given by Equation (7):

$$P_{24} = 47.38e^{-8.39\varepsilon}, \text{MPa}. \tag{7}$$

2.3. Numerical simulation

The numerical simulation by ANSYS was performed to analyze the behavior of SCDA in different strain modes and to create the SCDA model. The numerical model of experimental setup was made (Fig. 5a).

The specimen of SCDA was modeled as a solid cylinder with high (h) 40 mm and 40 mm in diameter, as in the laboratory experiment. During numerical experiment the outer diameter of the SCDA specimen and the outer diameter of piston corresponded to the inner diameter of the cylinder. There was no friction between the piston and the cylinder. There was no possibility of leaking expansion pressure in the simulation.

Thermal isotropic expansion model was used to simulate the behavior of SCDA by volumetric expands in hydration. The SCDA properties in the numerical model were calibrated, which made it possible to accurately simulate the expansion of the material. The calibration process consisted in changing of the secant coefficient of thermal expansion in order to achieve the minimal stress/strain error between the numerical model and the laboratory experiment. The resulting model describes the behavior of SCDA in all strain modes. Table 1 presents the SCDA properties that were assumed in the numerical simulation. The secant coefficient of thermal expansion as a result of calibration was 0.0018. The Poisson's ratio was 0.49, since the expansive process occurs as a result of a chemical reaction, which ensures the equal expansion pressure in all directions.

Fig. 5a also shows the result of a numerical calculation for a prestress of 29 MPa. As a result of volumetric expansion, the height of the SCDA specimen increased by $\Delta h = 2.66$ mm, which corresponds to a vertical strain value of 0.065 (2.66 mm/40 mm) (Fig. 5a), and it is close to the results of the laboratory experiment. In numerical simulation was used isotropic model, therefore the relationship of SCDA expansive pressure to strain was approximated linearly. At the same time, the fitting line connected the first and last points of the experimental data (Fig. 5b). The time parameter was set indirectly, through a change in temperature of SCDA model.

Table 2 shows the correspondence between the SCDA temperature in the model and the time of SCDA hydration in the laboratory test. The stepwise increase in temperature in the model (column 2 of Table 2) simulates the hydration reaction time (column 1 of Table 2), which corresponds to expansive pressure (column 3 of Table 2). Since the hydration process is exothermic, the temperature of the SCDA is a function of time. Thus, time is simulated by the indirect method. Fig. 5b shows the expansive pressure-strain curves that based on the results of numerical analysis for 3, 4, 5, 8, 24 h.

The ANSYS code was used to analyze the stress and strain state of rock around the SCDA hole. Two numerical models were established. Each model was 1 m × 1 m × 0.1 m in size and had one hole with the diameter 45 mm, as shown in Fig. 6. The model I

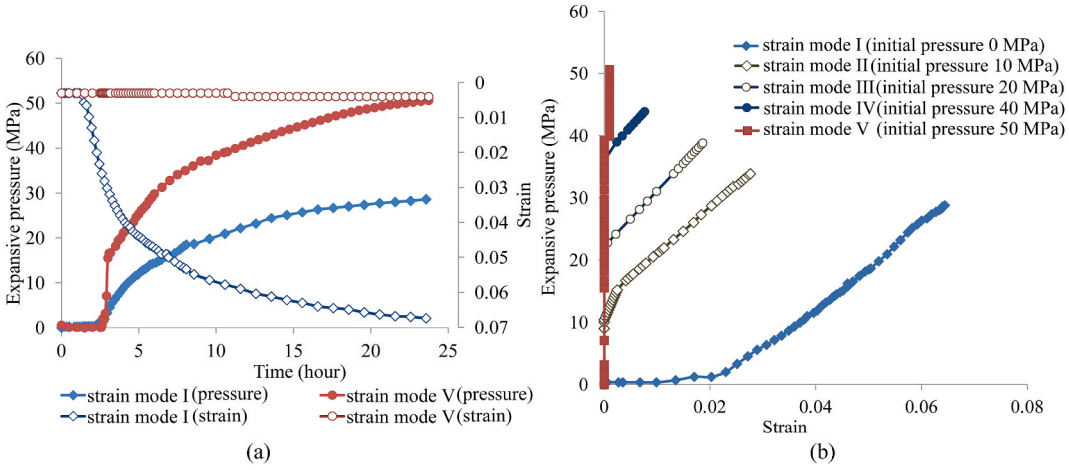

Fig. 4. Laboratory test results: (a) the evolutions of strain and expansive pressure produced by SCDA with max and min initial pressure; (b) relationships of SCDA expansive pressure to strain.

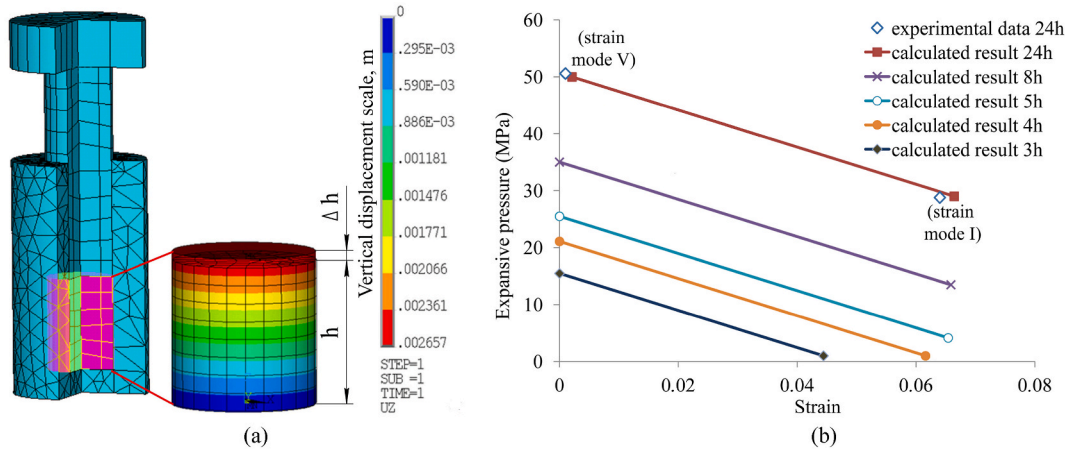

Fig. 5. Numerical model and its results: (a) the numerical model of experimental setup; (b) relationships of SCDA maximum expansive pressure to strain by different time.

Table 1
Properties of SCDA used in the model.

Type of element	Material behaviour option	Secant coefficient of thermal expansion	Thermal conductivity (W/m·K)	Elastic modulus (MPa)	Poisson's ratio
Solid	Isotropic termal expansion	0.0018	0.92	18.55	0.49

Table 2
Correspondence between lab time and temperature in the model.

Time in laboratory test, hour	Temperature in numerical simulation, °C	Expansive pressure by null strain, MPa
24	30	50.6
12	25	41.5
8	21	35.0
5	15	25.5
4	12	21.1
3	9	15.5
2	0	0.0

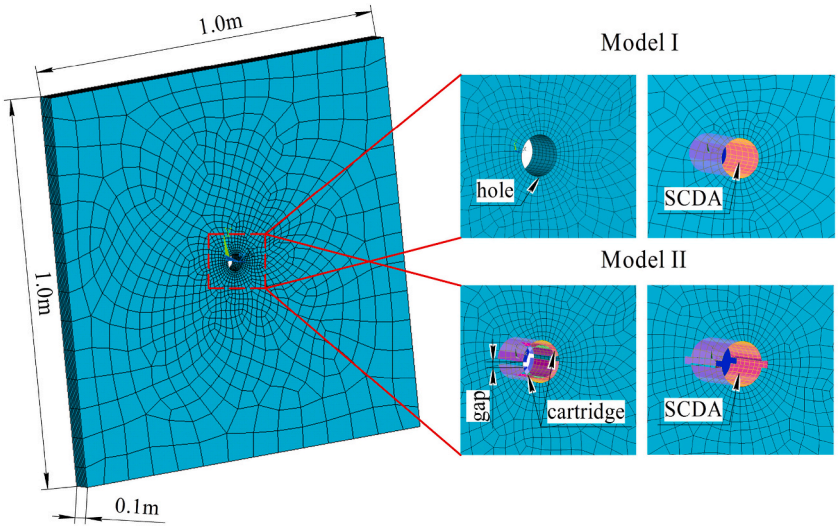

Fig. 6. Numerical model.

corresponded to the conventional rock fragmentation method by using SCDA. In this model, SCDA was placed inside the hole. In model II, a stress concentration cartridge was additionally installed and inside which SCDA was placed, as shown in Fig. 6. The gap between the elements of the cartridge during the simulations was varied from 0.45 to 0.75 mm. This range was chosen for reasons of cutting a slot in the pipe on the machine-tool with a milling cutter at a time. For all models horizontal displacements were fixed at the lateral boundaries, vertical displacements were fixed at the bottom and top boundaries. Near the hole, the size of the finite element was minimal, since high accuracy is important there. The minimum size of the finite element was 2.8 mm. On the contour of the model, the stress field is uniform, so the finite elements had the maximum size (up to 71.5 mm). The finite element grid was build by the automatic adaptive method within the given limits of accuracy. The minimum size was chosen in an iterative way, thus, to ensure maximum accuracy while avoiding the occurrence of an error in the calculation due to the zero length of the element after deforming.

Three types of rocks were used: granite, sandstone and mudstone, and their physical and mechanical parameters are shown in Table 3. The Linear Elastic and Drucker-Prager models were used to simulate the behavior of rocks. The element damage of rock was judged according to the maximum tensile stress criterion and the Mohr-Coulomb criterion [53]. The ultimate tension strength (σ_τ) of rocks is more than 10 times less than the ultimate compressive strength (σ_c), therefore the stress criterion is expressed by Equation (8):

$$\sigma_1 \leq [\sigma_\tau] \tag{8}$$

where σ_1 – maximum principal stress.

3. Results and discussion

3.1. Elastic numerical simulation

Many scientists use the elasticity theory for the analysis of stress fields that are formed by SCDA. Also, the elastic approach is often used in the calculation of fracture parameters [54–56]. At the first step of the current study elastic simulation was also used.

The stress distributions around the borehole with SCDA (model I) in the granite for hydration time 12 h are shown in Fig. 7. The increased maximum principal stresses σ_1 are formed in the shape of concentric circles, with an extremum near the hole surface, as shown in Fig. 7a. Minimum principal stresses σ_3 have a similar distribution, as shown in Fig. 7b. Thus, the uniform stress field is formed around the hole. The level of tensile stresses σ_1 near to the surface of hole is greater than the tensile strength of granite. Conditions for the initiation, and propagation of cracks are equal in all directions.

Fig. 8 shows the variation of maximum principle stress (σ_1) inside and nearby the borehole with SCDA along the monitoring line A-A^1. The monitoring line A-A^1 was arranged along the horizontal axis, from the center of hole to the deep. The stresses on this line increased with the SCDA hydration time, as shown in Fig. 8a. Fig. 8a shows that compressive stresses inside of the hole that are caused by SCDA expansion increase with hydration time. For example, when hydration time is 12 h, the expansive pressure in the hole is 41.26 MPa. In the immediate surroundings of the hole in the rock, compressive stresses σ_1 form. For example, in the granite after 12 h of SCDA hydration at a distance of 0.25 cm from the hole surface, σ_1 is −22 MPa, as shown in Fig. 8a.

A similar situation is observed in mudstone and sandstone, as shown in Fig. 8b. The expansive pressure of SCDA in mudstone and sandstone is less than in granite, since the deformation modulus of these rocks is lower, and therefore the strains are larger. The value of stress σ_1 around the SCDA hole in mudstone and sandstone does not differ much compared to granite, as shown in Fig. 8b.

The stress distributions around the borehole with SCDA and cartridge (model II) in granite for hydration time 12 h are shown in Fig. 9. The gap distance is 0.45 cm. Cartridges that are installed inside the hole significantly change the stress distribution in the rock. In this case the stress field is not uniform. Increased tensile stresses occur only in places that adjacent to the gap of the cartridge, as shown in Fig. 9. The zone of increased stresses is close in shape to an oval. In places of maximum principal stresses σ_1 concentration, the level of tensile stresses is much greater than the tensile strength of granite, as shown in Fig. 9a.

Minimum principal stresses σ_3 form regions of rock compression in the direction of the cartridge elements, and tensile stresses are formed in the gap of cartridge region, as shown in Fig. 9b. Conditions for the initiation, and propagation of cracks appear in this case only near the gap of the cartridge.

Fig. 10 shows the variation of maximum principle stress (σ_1) inside and nearby the borehole with SCDA and cartridge along the monitoring line B-B^1. The monitoring line B–B^1 was arranged from the center of hole through the middle of the gap of the cartridge to deep. Thus, the maximum tensile stresses are formed along this line. Fig. 10a shows that compressive stresses inside of the hole (that are caused by SCDA expansion) appear, similar to the model I. However, in this case, in the immediate surroundings of the hole, compressive stresses σ_1 do not arise. The extremum tensile stresses are formed on the hole surface, as shown in Fig. 10a. These stresses are more than 5 times higher than the maximum tensile stresses that were obtained in model I.

Stress distributions in mudstone and sandstone are similar, but the maximum principal stresses σ_1 on the hole surface and in its

Table 3
Rock properties.

Rock	Compressive strength, σ_c (MPa)	Tensile strength, σ_τ (MPa)	Deformation modulus (GPa)	Poisson's ratio	Cohesion value (MPa)	Angle of internal friction (°)	Dilatancy angle (deg)
Granite	98	16.2	67	0.25	30	46	46
Sandstone	56.3	5.14	25	0.25	10	38	38
Mudstone	25.8	1.31	0.9	0.25	4.64	32	32

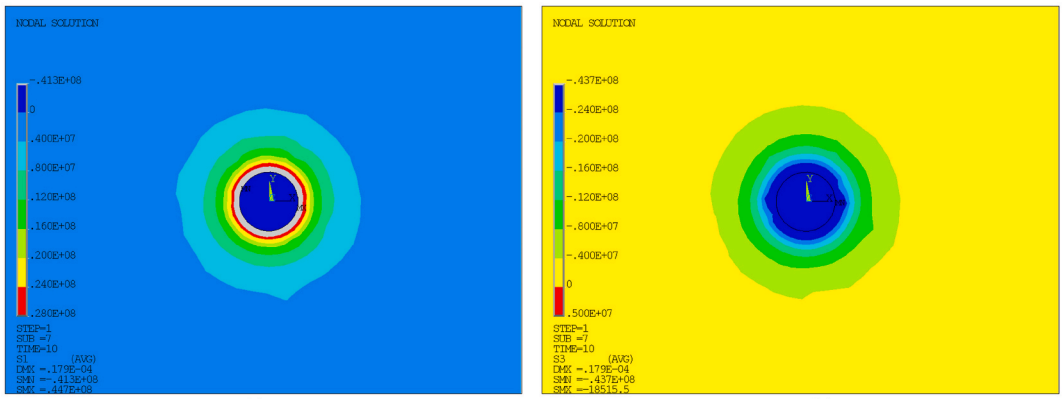

Fig. 7. The results of numerical calculation for model I: (a) distributions of maximum (σ_1) principal stresses; (b) distributions of minimum (σ_3) principal stresses.

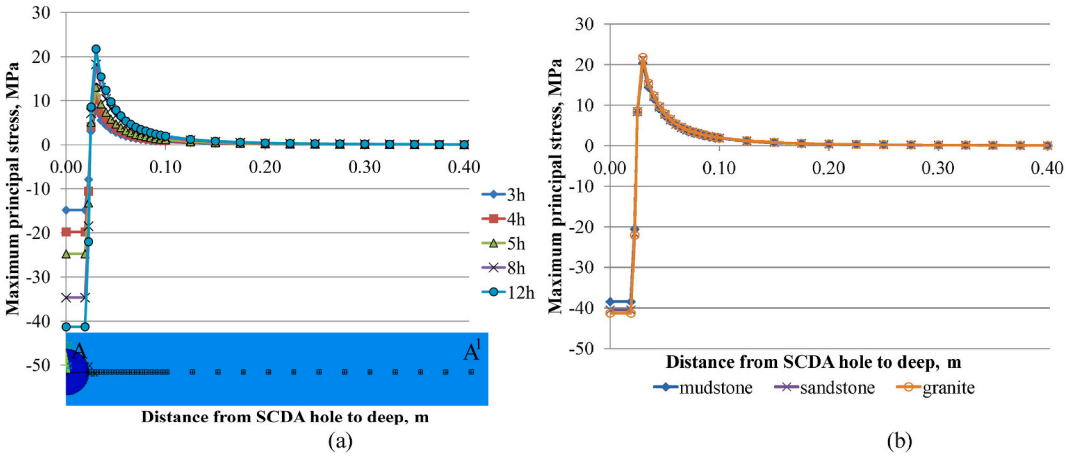

Fig. 8. Characteristics of maximum principle stresses (σ_1) on monitoring line A-A^1: (a) for granite with hydration time 3, 4, 5, 8, 12 h; (b) for mudstone, sandstone and granite with hydration time 12 h.

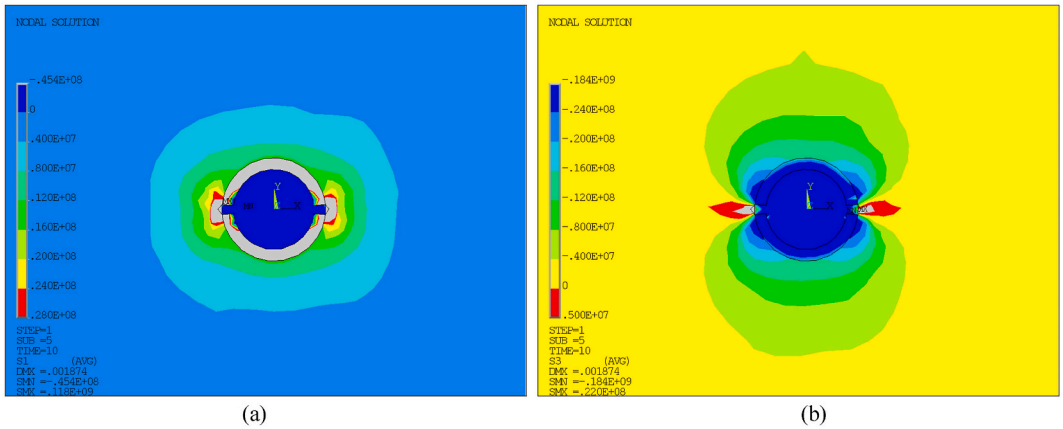

Fig. 9. The results of numerical calculation for model II: (a) distributions of maximum (σ_1) principal stresses; (b) distributions of minimum (σ_3) principal stresses.

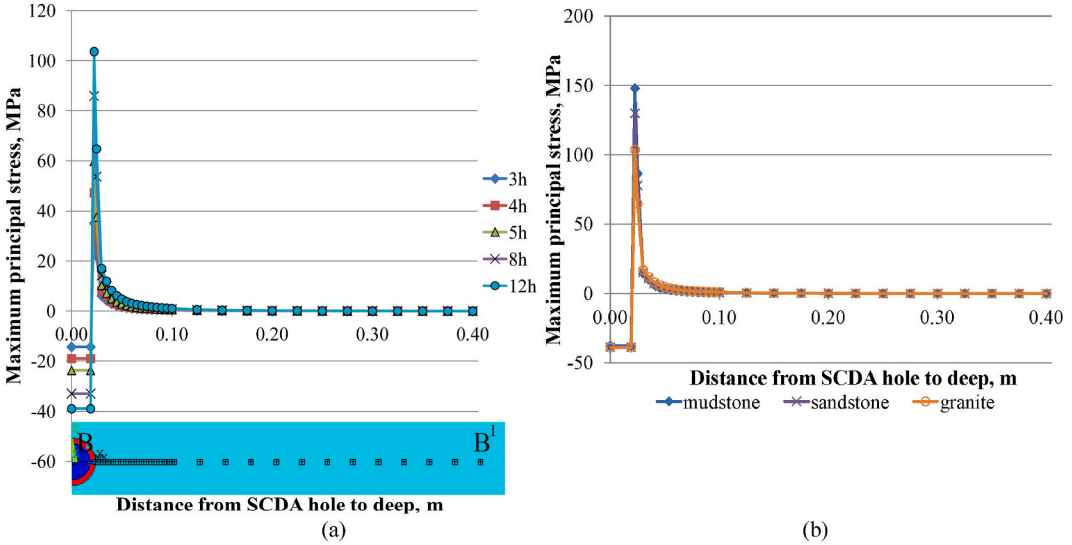

Fig. 10. Characteristics of maximum principle stresses (σ_1) on monitoring line B–B^1: (a) for granite with hydration time 3, 4, 5, 8, 12 h; (b) for mudstone, sandstone and granite with hydration time 12 h.

immediate surroundings are even higher than in granite, as shown in Fig. 10b. The effectiveness of using cartridges to control the site of crack initiation is clear.

The stress concentration in the proposed rock fracturing method by SCDA also depends on cartridge gap distance. Simulations were carried out to study the effect of this parameter. The studied gap distances are 0.45, 0.60, and 0.75 cm.

Fig. 11 shows the characteristics of maximum principle stresses (σ_1) along the monitoring line B-B^1 for model I and model II with different gap distance. The best effect is provided with a gap distance of 0.45 cm. While at a gap distance of 0.6 and 0.75 cm the maximum principal stresses do not differ significantly. Although the tensile stresses σ_1 on the hole contour for model II (with cartridge) are significantly higher than for model I (without cartridge). The absolute values of stress in mudstone are somewhat higher than in sandstone. However, the modeling results are qualitatively similar for sandstone (Fig. 11a) and mudstone (Fig. 11b). This suggests that the calculated maximum principle stresses variation is general regularity.

The stress concentration factor k_σ was defined as the stress σ_1 value at that point in model II divided by the stress σ_1 value for model I. For SCDA hydration time 12 h the stress concentration factor is presented in Fig. 12. In the model I the stresses σ_1 nearby the hole are compressive, while in model II they are tensile, therefore the stress concentration factor in this region has a negative sign. For considered types of rocks, the minimum cartridge gap distance provides the maximum stress concentration, what is generally logical. An increase in the gap distance leads to a decrease in the stress concentration factor k_σ. For example, for granite (Fig. 12a) the maximum stress concentration factor is 5.51, 5.76, 7.56 with a cartridge gap distance of 0.75, 0.6 and 0.45 cm. In addition, the maximum effect from the applying of cartridges is typical for mudstone, which has the minimum deformation modulus among the compared rocks. So for granite, the stress concentration factor with a gap distance of 0.45 cm is 7.56 (Fig. 12a), for sandstone it is 9.23 (Fig. 12b), and for mudstone it is 10.67 (Fig. 12c).

The stress concentrations (mentioned above) are localized at a distance of up to 1 cm from the hole contour. In this region the formation of cracks occurs. To evaluate the effectiveness of the use of cartridges, the parameter a/d was proposed, where (a) is the

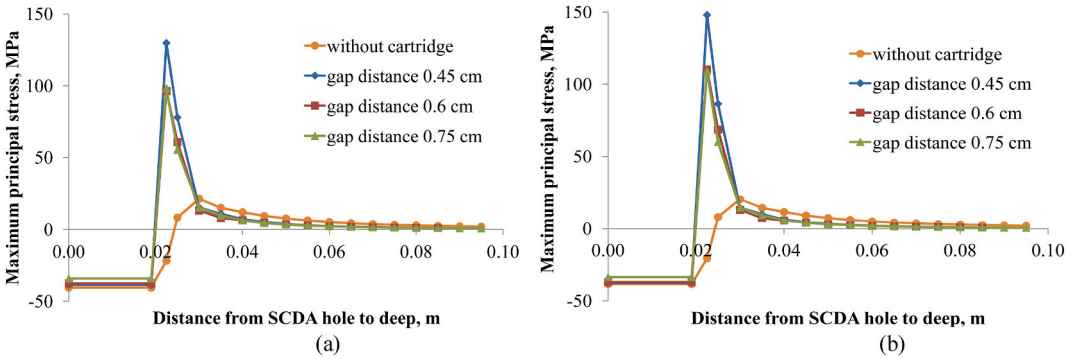

Fig. 11. Characteristics of maximum principle stresses (σ_1) on monitoring line B–B^1 by different gap distance: (a) sandstone; (b) mudstone.

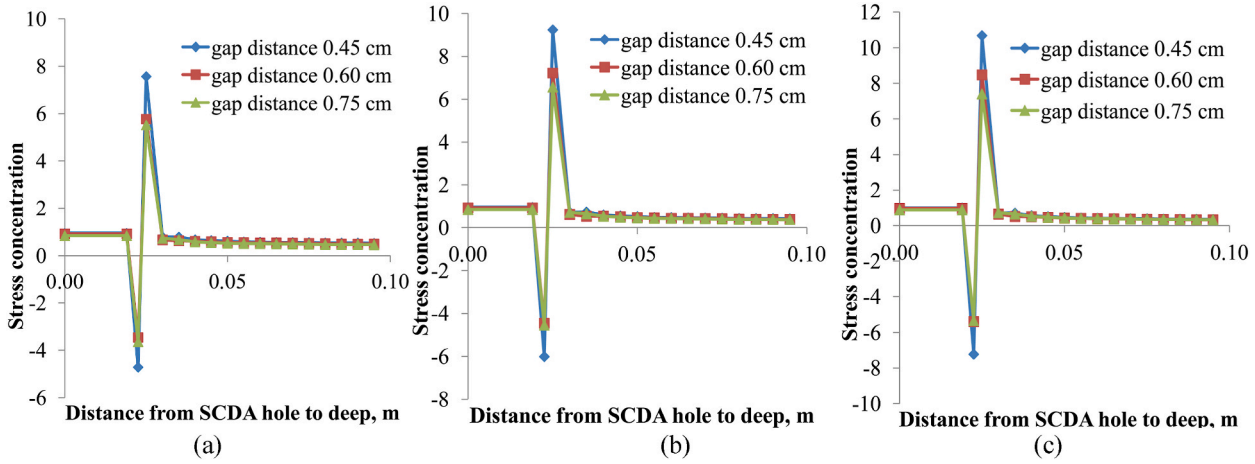

Fig. 12. Characteristics of stress concentration factor on monitoring line B–B[1] with different gap distance: (a) granite; (b) sandstone; (c) mudstone.

cartridge gap distance, (d) is the diameter of the hole. Relationship of stress concentration factor to a/d parameter is shown in Fig. 13.

3.2. *In-situ verification of calculated results for linear elastic model*

Equation (5) (proposed by Sakhno et al. [9]) was used to calculate the borehole spacing. The following values of variables were accepted: expansive pressure P, typical for the SCDA hydration time of 12 h (Table 2); values E_r according to Table 3; $r_0 = 0.02$ m; $\mu_{SCDA} = 0.48$; $K_I = 1.0$ MN/m$^{3/2}$.

The elastic modulus of SCDA is not a constant; it depends on the strain of rocks. E_{SCDA} is determined by dividing the expansive pressure P by the SCDA strain.

The results of numerical simulation were used to calculate E_{SCDA}. So the displacement of SCDA in the diametrical direction of the hole with a hydration time of 12 h was 0.000182 m, 0.000608 m, 0.0021 m for granite, sandstone and mudstone, respectively. The expansive pressure inside the hole was 41.3 MPa, 40.2 MPa, and 36.4 MPa, respectively. Based on the obtained results, the strain of rocks and E_{SCDA} were calculated. The calculated minimum hole spacing was 0.31 m, 0.38 m, 0.43 m for granite, sandstone and mudstone respectively.

For the proposed rock fracturing method, equation (5) can be modified as:

$$L_{cr} = k_\sigma \frac{3P^2 \times \pi \times r_0^2 \times E_r}{8E_{SCDA} \times K_I^2}(1 - 2\mu_{SCDA}), \tag{9}$$

where:

k_σ – stress concentration factor.

Verification of the results of numerical simulation was carried out during the fracturing of oversized blocks of granite and sandstone, which were formed as a result of drilling and blasting. The fracturing of granite was carried out under the conditions of the Khlebodarovsky quarry in Ukraine. According to geological department data, in experimental block the compressive strength of granite in air-dry state was 98 MPa, tensile strength was 16.25 MPa. The fracturing sandstone experiments were in the conditions of the mine Shcheglovskaya Glubokaya in Ukraine. According to the geological report, sandstone uniaxial compressive strength was 56.3 MPa, tensile strength was 5.14 MPa.

For the test 4 blocks of granite and 4 blocks of sandstone were selected for fracturing by conventional method. The hole spacing, that was calculated by equation (5), for the fracturing of granite without a cartridge, was 31 cm, the real distance in-site was 30 cm.

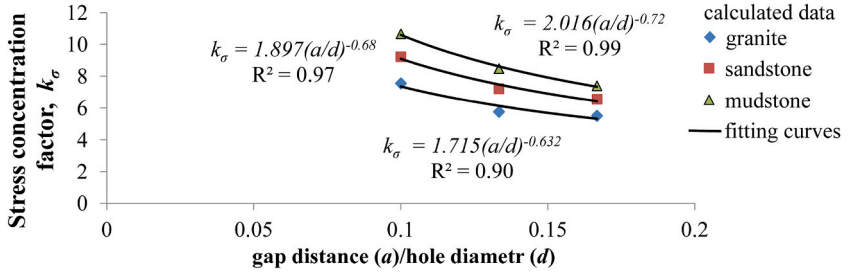

Fig. 13. The relationships of stress concentration factor to a/d parameter for granite, sandstone and mudstone.

The actual hole spacing in the sandstone was 38 cm, which coincided with the calculated one. The hole diameter was 0.40 cm.

Preparation for the fracturing of rocks with SCDA by conventional method and the results of the fracturing are shown in Fig. 14. Fig. 14a shows the process of pouring SCDA into holes in granite block. SCDA mixture that was poured into boreholes in sandstone in coal mine shows in Fig. 14c. The experiment showed that all blocks of granite (Fig. 14b) and sandstone (Fig. 14d) were destroyed. Equation (5) makes it possible to adequately calculate the hole spacing.

The calculation of the hole spacing according to equation (9) showed that during the fracturing of granite with the cartridge gap distance 0.4 cm (parameter a/d = 0.1) stress concentration factor $k_\sigma = 7.56$ (Fig. 13), and $L_{cr} = 2.34$ m. So, blocks of granite with a length of less than 2.34 m should theoretically be destroyed by one borehole with SCDA. For the test, 4 blocks of granite were selected. The blocks had a length of 1.18 m, 1.35 m, 1.5 m, 1.65 m, and 1 hole was drilled in each of them. The cartridge gap distance was controlled by installing a metal plate with thickness of 0.4 cm between the parts of the cartridge in its upper, middle and lower parts. Fig. 15 shows the process of preparing and installing SCDA cartridges into boreholes. Fig. 15a shows the process of pouring SCDA mixture into the cartridge element before installing the cartridge into hole in granite block. The volume of the SCDA that was filled in each 1 m of boreholes was 2.2 L. The general view of cartridge with SCDA after installation is shown in Fig. 15b. However, the results were unsatisfactory even when the blocks sizes were much smaller than the calculated ones. None of the granite blocks with hole spacing that was calculated by equation (9) was destroyed, as shown in Fig. 16. The main crack did not occur in the block of minimum dimensions (Fig. 16a) but in the block of maximum dimensions (Fig. 16b). The results of SCDA fracturing of sandstone blocks with the proposed method were also unsatisfactory.

Since equation (5) gives adequate hole spacing for the fracturing by the conventional method and equation (9) differs from it by adding a stress concentration factor (in proposed method), the error clearly consists in estimating of the stress concentration.

So, the results of the in-situ tests showed that the more thorough assessment of the value of the stress concentration factor is needed. It was concluded that elastic numerical model which was used to determine the stress concentration factor does not allow obtaining reliable results confirmed by practice.

Fig. 14. Experiments in-situ: (a) pouring SCDA mixture into boreholes in granite; (b) fracturing of granite by conventional SCDA method; (c) pouring SCDA mixture into boreholes in sandstone; (d) fracturing of sandstone by conventional SCDA method.

Fig. 15. Preparation to fracturing of granite by proposed SCDA method: (a) pouring SCDA mixture into the cartridge; (b) cartridge with SCDA after installation.

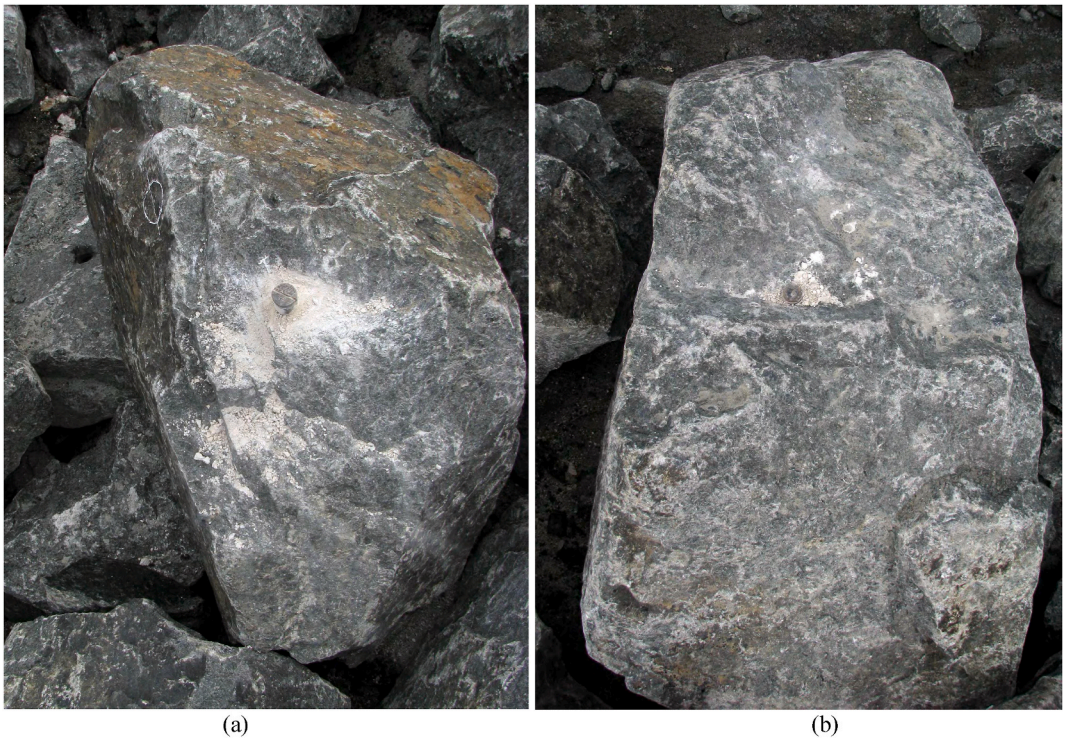

Fig. 16. Unsuccessful results of granite fracturing by proposed SCDA method: (a) block with minimum length; (b) block with maximum length.

3.3. Non-elastic numerical simulation

The linear elastic model turned out to be incorrect, since its results have not been confirmed by in situ experiments; therefore the Drucker-Prager model was used at the second step of the current study.

The stress distributions around the borehole with SCDA (model I) in granite, sandstone and mudstone for hydration time 12 h for Linear Elastic and Drucker-Prager Models are shown in Fig. 17. In the elastic model, there are no significant differences in the distributions of stresses for different rock types, as shown in Fig. 17 a. However, such differences are significant in case of using the Drucker-Prager model, as can be seen from Fig. 17 b. The more the plastic properties in the rock characterized, the greater the zone of

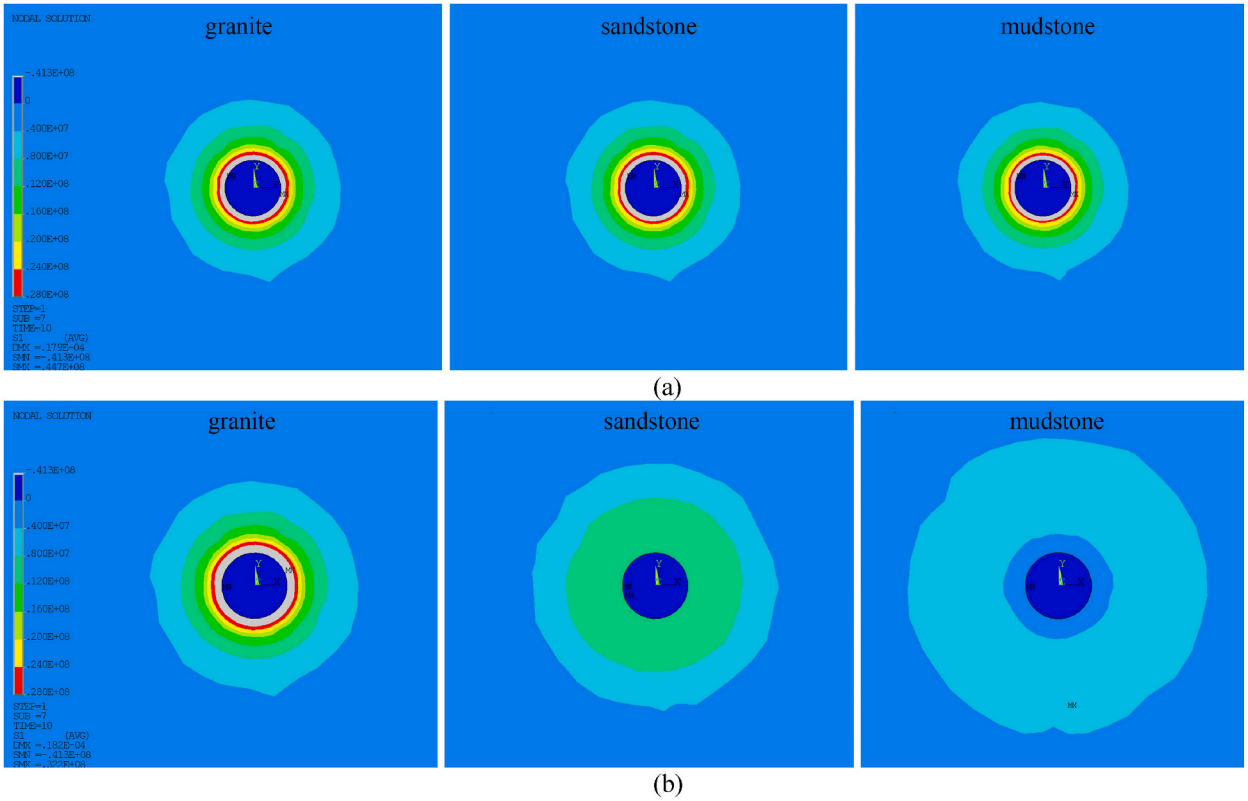

Fig. 17. The stress distributions around the borehole with SCDA (model I) for hydration time 12 h: (a) Linear Elastic model; (b) Drucker-Prager model.

influence of the hole with the SCDA. Differences are typical for sandstone and mudstone. The rock compression zone increases around the SCDA hole for these rocks. At the same time, the value of maximum principal stresses σ_1 is noticeably smaller than in elastic model, which is explained by the transition of the rock to the plastic stage of deformation. For granite, which is highly brittle, there is no difference between plastic and elastic numerical calculations because the elastic limit of granite is not exceeded.

Fig. 18 shows the distributions of maximum principle stresses (σ_1) inside and nearby the borehole with SCDA along the monitoring line A-A[1]. Since the stress distribution for granite does not differ from the elastic model (Fig. 8a), so the characteristics of maximum principle stress for sandstone are shown in Fig. 18a.

An increase in expansion pressure leads to the increase in the tensile stress region in the sandstone, while the stress value does not increase more than 10.9 MPa, that is limited by the elastic limit, as shown in Fig. 18a. In the immediate surroundings of the hole, compressive stresses σ_1 appear in the rock. The radius of the compression zone is larger than in the elastic model.

As mentioned above, the stress distribution in granite, mudstone and sandstone is different. The value of the principle stresses σ_1 nearby the SCDA hole depends on the elastic limit of the rocks, it is maximum for granite, and minimum for mudstone, as shown in Fig. 18b. In this case, peak stresses appear in granite, which is characteristic of the elastic behavior of the material, while in sandstone and mudstone, the deformation curve describes the plastic behavior of rocks in the near-hole region.

The stress pattern nearby the hole with SCDA and cartridge (the gap distance is 0.45 cm) in granite, sandstone and mudstone for hydration time 12 h for Linear Elastic and Drucker-Prager Models are shown in Fig. 19. The stress fields vary insignificantly in the case of the elastic model for different rock types. When the Drucker-Prager model was used, the value of maximum stresses and the shape of the zone of hole influence are various for different rock types. For granite, the stress pattern is similar to the obtained one in the case of the elastic model. For sandstone and mudstone, the tensile stress zone has an other shape (not an oval). The maximum principal stresses σ_1 are smaller than the obtained ones in the elastic model. Tensile stresses σ_1 are concentrated mainly near the gap of the cartridge,as shown in Fig. 19b. In places of maximum principal stresses σ_1 concentration the level of tensile stresses is greater than the tensile strength of rocks. In these regions the conditions for the cracks initiation appear.

Fig. 20 shows the distributions of maximum principle stress (σ_1) inside and nearby the borehole with SCDA along the monitoring line B–B[1]. Fig. 20a shows the characteristics of maximum principle stress for sandstone. The increase in expansive pressure leads to the growth of the tensile stress σ_1 region in the sandstone. At the same time the stress value does not increase more than 12.92 MPa. So stress σ_1 is more than 10 times less, compared with the elastic model, as shown in Fig. 20a. The zone of increased σ_1 is more than 2 times larger.

Installation of the cartridge does not change significantly the stress pattern in granite. However plastic deformations appear near

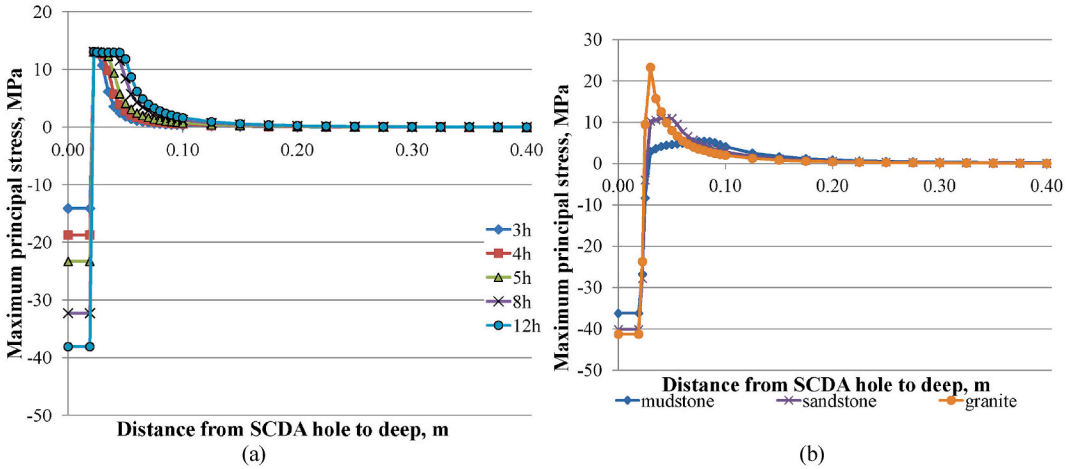

Fig. 18. Characteristics of maximum principle stresses (σ_1) on monitoring line A-A[1]: (a) for sandstone with hydration time 3, 4, 5, 8, 12 h; (b) for mudstone, sandstone and granite with hydration time 12 h.

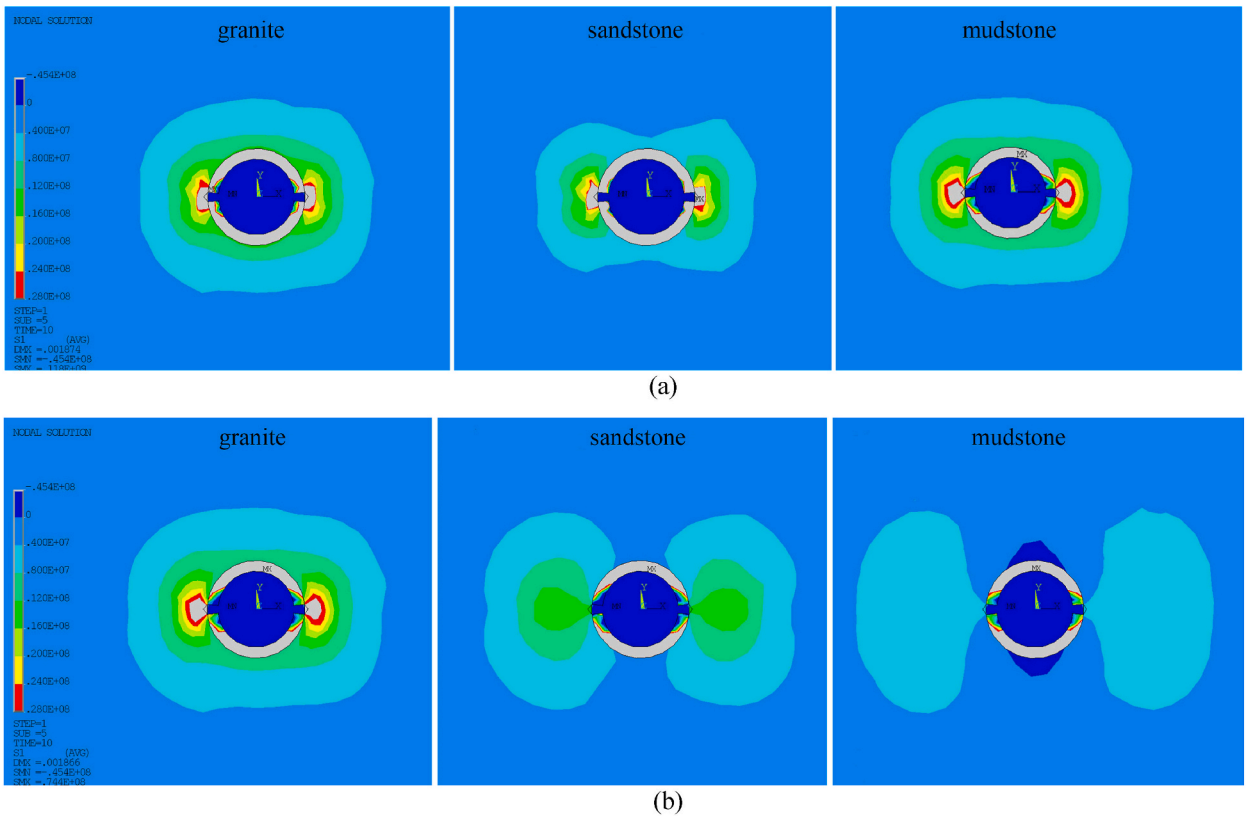

Fig. 19. The stress distributions around the borehole with SCDA (model II) for hydration time 12 h (gap distance is 0.45 cm): (a) Linear Elastic model; (b) Drucker Prager model.

the hole and the value of σ_1 peak is three times less than in the elastic model (Fig. 20b). The extremum tensile stresses are more than 2.0, 2.5, 5.4 times higher than the tensile strength for granite, sandstone and mudstone respectively. The condition for crack initiation according to the maximum tensile stress criterion is fulfilled.

Fig. 21 shows the characteristics of maximum principle stress (σ_1) along the monitoring line B-B[1] for model I and model II with different gap distance. The best effect is achieved with the gap distance of 0.45 cm, although the difference in maximum stresses is insignificant, in opposite to the elastic model. The difference between the tensile stresses σ_1 on the hole surface for model II (with

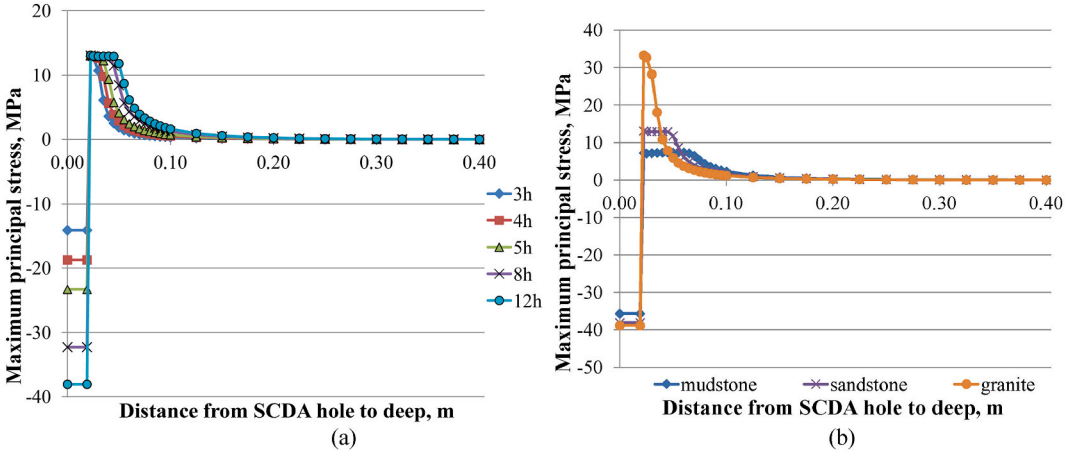

Fig. 20. Characteristics of maximum principle stress (σ_1) on monitoring line B–B^1: (a) for sandstone with hydration time 3, 4, 5, 8, 12 h; (b) for mudstone, sandstone and granite with hydration time 12 h.

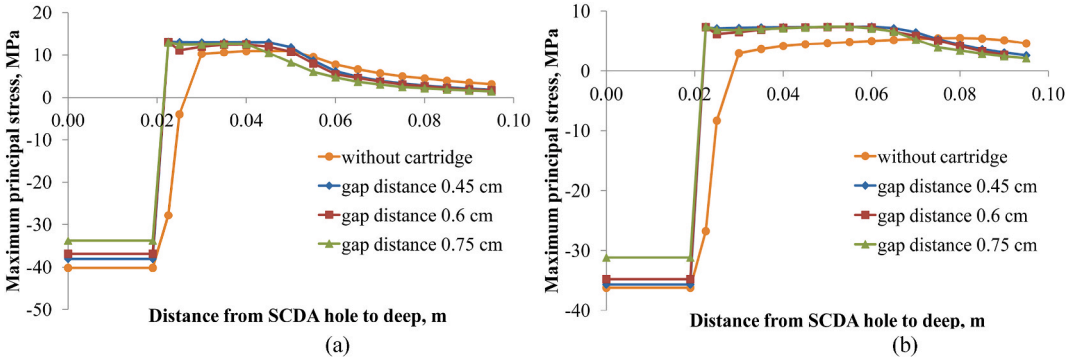

Fig. 21. Characteristics of maximum principle stress (σ_1) on monitoring line B–B^1 by different gap distance: (a) sandstone; (b) mudstone.

cartridge) and model I (without cartridge) is not large. At the same time, the maximum principle stress on the contour of the hole with the cartridge in sandstone is 12.93 MPa (Fig. 21a), and in mudstone it is 7.43 MPa (Fig. 21b).

The stress concentration factor for SCDA hydration time 12 h is presented in Fig. 22. For all considered types of rocks, the minimum gap distance provides the maximum stress concentration. However, the difference in the stress concentration factor is not significant, compared with the elastic model. The maximum effect is achieved in granite. For example, for granite with a gap distance of 0.45, 0.6

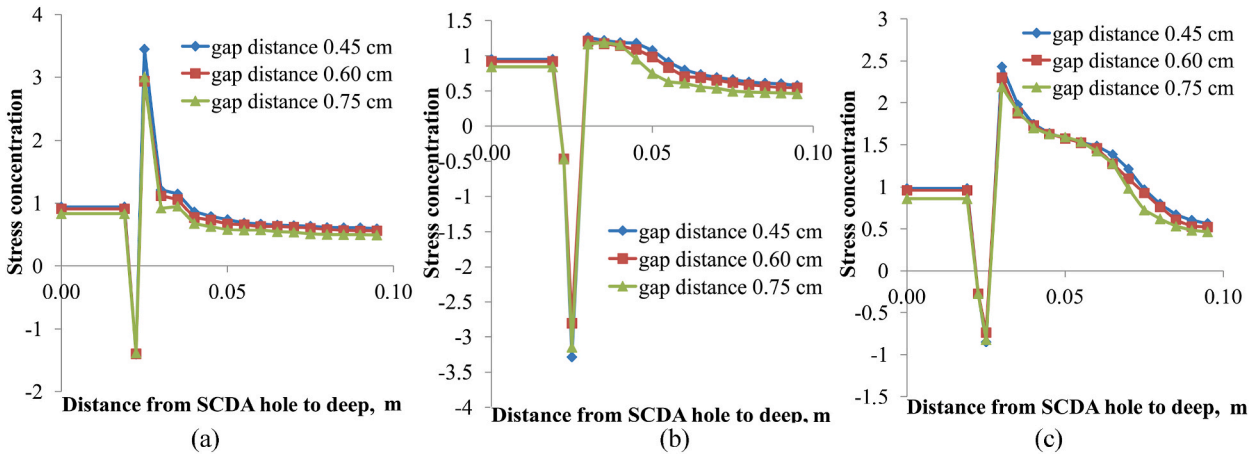

Fig. 22. Characteristics of stress concentration factor on monitoring line B–B^1 by different gap distance: (a) granite; (b) sandstone; (c) mudstone.

and 0.75 cm, the maximum stress concentration factor is 3.45, 3.0, 2.93 respectively (Fig. 22a), for mudstone it is 2.43. 2.3. 2.19 respectively (Fig. 22c), while for sandstone stress concentration factor is 1.26, 1.21, and 1.17 respectively (Fig. 22b).

The stress concentration factor variation from parameter a/d for different rock types is shown in Fig. 23. Clearly, the effectiveness of cartridges installation in the case of using Drucker-Prager model much lower compared with linear elastic model.

3.4. In-situ verification of calculated results for Drucker-Prager model

Verification of the numerical simulation results was carried out under the conditions that were described above in paragraph 3.2. The calculation of the stress concentration factor according to Fig. 23 showed that with the parameter $a/d = 0.1$ (cartridge gap distance is 0.04 cm), k_σ for granite is 3.45, and k_σ for sandstone is 1.26. The minimum hole spacing that was determined by equation (9) for the fracturing of granite was 1.06 m, and for sandstone was 0.47 m.

For the test, 4 blocks of granite and 2 blocks of sandstone were selected. The blocks had a length of 1.05 m, 0.95 m, 0.92 m, 0.87 m, and 1 hole was drilled in each of them. The hole spacing in the sandstone was 0.45 cm. All blocks that were selected for the experiment were fractured. Fig. 24a and b shows preparation of granite and sandstone blocks for SCDA pouring. The initiation of main cracks nearby SCDA holes in granite and sandstone is shown in Fig. 24c and d. The fractured rocks are shown in Fig. 24e and f.

In-situ experiments confirmed the effectiveness of the proposed directional fracturing method. The correctness of calculation of the stress concentration factor was also confirmed. The proposed method for calculating the hole spacing has been tested and proven to be accurate. In the future, our efforts will be focused on improving of the technology of directional fracturing for the possibility of a wider industrial application.

4. Conclusions

In this study, non-explosive directional fracturing of rock was considered as the research subject. We focused on the SCDA rock fracturing mechanism and the effectiveness of using of the proposed stress concentration cartridges. The numerical simulation was used to study the stress distributions nearby the borehole with SCDA in different rock types in the case of conventional and proposed fracturing method. The results demonstrated that cartridge installation leads to significant change of stress distribution around of the hole. As a result, it becomes possible to create a directional fracturing of rocks. This was followed by investigating of the effectiveness of directional fracturing with stress concentration cartridges. Based on the results of this investigation, the following conclusions can be drawn.

(1) The numerical analysis shows that the installation of cartridge inside the borehole significantly changes the stress distribution nearby the hole. In this case the stress field in rock is not uniform. Tensile stress concentrations occur only near to the gap of the cartridge. In-situ experiments show that the linear elastic model is incorrect for describing stress-strain state of rock. The Drucker-Prager model describes the behavior of rocks quite accurately and the simulation results are confirmed by in-situ experiments. The value of the principle stresses nearby the hole with SCDA depends on the elastic limit of the rocks; it is maximum for granite, and minimum for mudstone. In places of maximum principal stress concentrations the level of tensile stress significantly exceed the tensile strength of rocks that cause the initiation and propagation of cracks.

(2) The value of tensile stress concentration in the proposed rock fracturing method significantly depends on a cartridge gap distance. To evaluate the effectiveness of the use of cartridges, the parameter a/d was proposed, where (a) is the cartridge gap distance, (d) is the diameter of the hole. For granite, sandstone and mudstone, relationships of stress concentration factor to a/d parameter were obtained with a correlation coefficient R^2 of more than 0.9. The results of the study are confirmed by experiments in-situ on the directional fracturing of rocks in a quarry and in a coal mine. This can provide suggestions for the specific parameters suitable for directional rock fracturing through SCDA technology.

Recommendations for further research.

Future studies will be aimed at measure existing minor crack after drilling and after SCDA fracturing, generated crack lengths and it growth rate. A SWOT analysis and cost benefit analysis (CBA) of explosive and non-explosive fracturing methods will also be conducted.

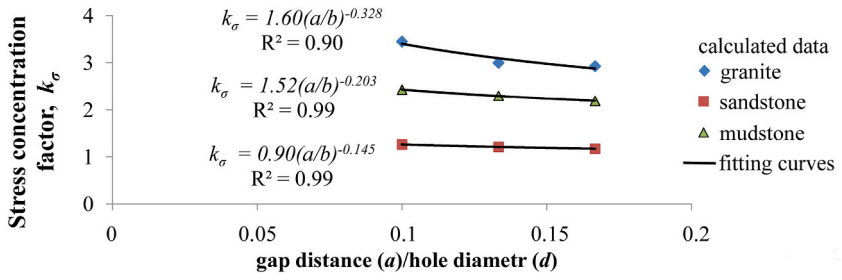

Fig. 23. The relationships of stress concentration factor to a/d parameter for granite, sandstone and mudstone.

Fig. 24. Rock fracturing by proposed SCDA method: (a, b) preparation to fracturing; (c, d) crack initiation; (e, f) result of fracturing.

Funding

This research received no external funding.

Data availability statement

Specific data is not used in this study. The results of numerical modeling were used to create some figures. These data will be made available on request.

Additional information

No additional information is available for this paper.

CRediT authorship contribution statement

Ivan Sakhno: Writing – original draft, Visualization, Supervision, Methodology, Investigation, Conceptualization. **Svitlana Sakhno:** Writing – review & editing, Visualization, Validation, Software, Investigation, Formal analysis.

Declaration of competing interest

The authors declare that they have no known competing financial interests or personal relationships that could have appeared to influence the work reported in this paper.

References

[1] K. Fuławka, L. Stolecki, P. Mertuszka, M. Szumny, A. Anderko, Predictive model of seismic vibrations' peak value induced by multi-face blasting, Journal of Sustainable Mining 22 (3) (2023) 7, https://doi.org/10.46873/2300-3960.1390.

[2] J.D. Armaghani, T.E. Mohamad, M. Hajihassani, A.N.S. K Abad, A. Marto, M.R. Moghaddam, Evaluation and prediction of flyrock resulting from blasting operations using empirical and computational methods, Eng. Comput. 32 (1) (2016) 109–121, https://doi.org/10.1007/s00366-015-0402-5.

[3] M. Monjezi, M. Hasanipanah, M. Khandelwal, Evaluation and prediction of blast-induced ground vibration at Shur River Dam, Iran, by artificial neural network, Neural Comput. Appl. 22 (2013) 1637–1643, https://doi.org/10.1007/s00521-012-0856-y.

[4] Y. Dai, M. Khandelwal, Y. Qiu, J. Zhou, M. Monjezi, P. Yang, A hybrid metaheuristic approach using random forest and particle swarm optimization to study and evaluate backbreak in open-pit blasting, Neural Comput. Appl. 34 (2022) 6273–6288, https://doi.org/10.1007/s00521-021-06776-z.

[5] U. Andres, Development and prospects of mineral liberation by electrical pulses, Int. J. Miner. Process. 97 (2010) 31–38, https://doi.org/10.1016/j.minpro.2010.07.004.

[6] M.R. Seyed, R. Bahram, I. Mehdi, H.R. Mohammad, Numerical simulation of high voltage electric pulse comminution of phosphate ore, Int. J. Min. Sci. Technol. 25 (2015) 473–478, https://doi.org/10.1016/j.ijmst.2015.03.023.

[7] C. Li, L. Duan, S. Tan, V. Chikhotkin, X. Wang, An electro breakdown damage model for granite and simulation of deep drilling by high-voltage electropulse boring, Shock Vib. (1) (2019) 1–12, https://doi.org/10.1155/2019/7149680.

[8] C. Li, L. Duan, S. Tan, V. Chikhotkin, W. Fu, Damage model and numerical experiment of high-voltage electro pulse boring in granite, Energies (2019) 12, https://doi.org/10.3390/en12040727.

[9] S. Walsh, D. Vogler, Simulating electropulse fracture of granitic rock, Int. J. Rock Mech. Min. Sci. 128 (2020) 104238, https://doi.org/10.1016/j.ijrmms.2020.104238.

[10] S.V. Serdyukov, M.V. Kurlenya, A.V. Patutin, et al., Experimental test of directional hydraulic fracturing technique, J. Min. Sci. 52 (4) (2016) 615–622, https://doi.org/10.1134/S1062739116040998.

[11] J.Q. Deng, C. Lin, Q. Yang, et al., Investigation of directional hydraulic fracturing based on true tri-axial experiment and finite element modeling, Comput. Geotech. 75 (2016) 28–47, https://doi.org/10.1016/j.compgeo.2016.01.018.

[12] W.Y. Lu, C.C. He, Numerical simulation of the fracture propagation of linear collaborative directional hydraulic fracturing controlled by pre-slotted guide and fracturing boreholes, Eng. Fract. Mech. 235 (2020) 107128, https://doi.org/10.1016/j.engfracmech.2020.107128.

[13] Y.G. Cheng, Z.H. Lu, X.D. Du, et al., A crack propagation control study of directional hydraulic fracturing based on hydraulic slotting and a nonuniform pore pressure field, Geofluids 2020 (2020) 1–13, https://doi.org/10.1155/2020/8814352.

[14] E.C. Donaldson, W. Alam, N. Begum, Hydraulic Fracturing Explained: Evaluation, Implementation, and Challenges, Elsevier, Amsterdam, The Netherlands, 2014.

[15] W.L. Ellsworth, Injection-induced earthquakes, Science 341 (6142) (2013) 1225942, https://doi.org/10.1126/science.1225942.

[16] A.A. Holland, Earthquakes triggered by hydraulic fracturing in south-central Oklahoma, Bull. Seismol. Soc. Am. 103 (2013) 1784–1792, https://doi.org/10.1785/0120120109.

[17] S.G. Osborn, A. Vengosh, N.R. Warner, R.B. Jackson, Methane contamination of drinking water accompanying gas-well drilling and hydraulic fracturing, Proc. Natl. Acad. Sci. USA 108 (2011) 8172–8176, https://doi.org/10.1073/pnas.1100682108.

[18] W. Wanniarachchi, P. Ranjith, M. Perera, A. Lashin, N. Al Arifi, J. Li, Current opinions on foam-based hydro-fracturing in deep geological reservoirs, Geomech. Geophys. Geo-Energy Geo-Resour. 1 (2015) 121–134, https://doi.org/10.1007/s40948-015-0015-x.

[19] V.R.S. De Silva, P.G. Ranjith, M.S.A. Perera, B. Wu, T.D. Rathnaweer, A modified, hydrophobic soundless cracking demolition agent for non-explosive demolition and fracturing applications, Process. Saf. Environ. 119 (2018) 1–13, https://doi.org/10.1016/j.psep.2018.07.010.

[20] A. Natanzi, D. Laefer, S. Zolanvari, Selective demolition of masonry unit walls with a soundless chemical demolition agent, Construct. Build. Mater. 248 (2020) 118635, https://doi.org/10.1016/j.conbuildmat.2020.118635.

[21] V.R.S. De Silva, P.G. Ranjith, Evaluation of injection well patterns for optimum fracture network generation host-rock formations: an application in in-situ leaching, Miner. Eng. 137 (2019) 319–333, https://doi.org/10.1016/j.mineng.2019.04.008.

[22] S. Wu, C. Zhai, J. Xu, L. Qin, Y. Sun, R. Dong, The performance of soundless cracking agents for weakening rock roof under different notch angles, Arabian J. Geosci. 12 (11) (2019) 1–13, https://doi.org/10.1007/s12517-019-4522-x.

[23] S. Sakhno, B. Kobylianskyi, I. Sakhno, Destruction of rocks by the non-explosive depleting compounds during mining, Mining of Mineral Deposits 10 (1) (2016) 25–30, https://doi.org/10.15407/mining10.01.025.

[24] T. Guo, S. Zhang, H. Ge, Z. Qu, A novel "soundless cracking agent fracturing" for shale gas reservoir stimulation, Int. J. Environ. Sustain Dev. 6 (9) (2015) 681–687, https://doi.org/10.7763/IJESD.2015.V6.680.

[25] V.R.S. De Silva, P.G. Ranjith, M.S.A. Perera, An alternative to conventional rock fragmentation methods using SCDA: a review, Energies 9 (11) (2016) 958, https://doi.org/10.3390/en9110958.

[26] T. Harada, K. Soeda, T. Idemitsu, A. Watanabe, Characteristics of Expansive Pressure of an Expansive Demolition Agent and the Development of New Pressure Transducers, vol. 478, Doboku Gakkai Rombun-Hokokushu/Proceedings of the Japan Society of Civil Engineers, 1993, pp. 95–109, https://doi.org/10.2208/jscej.1993.478_91.

[27] S. Arshadnejad, K. Goshtasbi, J. Aghazadeh, A model to determine hole spacing in the rock fracture process by non-explosive expansion material, Int. J. Miner. Metall. Mater. 18 (5) (2011) 509–514, https://doi.org/10.1007/s12613-011-0470-5.

[28] A.S. Natanzi, D.F. Laefer, L. Connolly, Cold and moderate ambient temperatures effects on expansive pressure development in soundless chemical demolition agents, Construct. Build. Mater. 110 (2016) 117–127, https://doi.org/10.1016/j.conbuildmat.2016.02.016.

[29] J. Hinze, J. Brown, Properties of soundless chemical demolition agents, J. Construct. Eng. Manag. 120 (4) (1994) 816–827, https://doi.org/10.1061/(asce)0733-9364(1994)120:4(816).

[30] D. Laefer, A. Natanzi, S. Zolanvari, Impact of thermal transfer on hydration heat of a soundless chemical demolition agent, Construct. Build. Mater. 187 (2018) 348–359, https://doi.org/10.1016/j.conbuildmat.2018.07.168.

[31] J. Hinze, A. Nelson, Enhancing performance of soundless chemical demolition agents, J. Construct. Eng. Manag. 122 (2) (1996) 193–195, https://doi.org/10.1061/(ASCE)0733-9364(1996)122:2(193).

[32] M.P. Huynh, D.F. Laefer, J. McGuill, A. White, Temperature related performance factors for chemical demolition agents, Int. J. Masonry Res. Inn. 2 (2–3) (2017) 220–240, https://doi.org/10.1504/IJMRI.2017.085952.

[33] A. Dessouki, H. Mitri, Rock breakage using expansive cement, Engineering 3 (2) (2011) 168–173, https://doi.org/10.4236/eng.2011.32020.
[34] M. Heikal, Effect of calcium formate as an accelerator on the physicochemical and mechanical properties of pozzolanic cement pastes, Cement Concr. Res. 34 (6) (2004) 1051–1056, https://doi.org/10.1016/j.cemconres.2003.11.015.
[35] M.C.G. Juenger, P.J.M. Monteiro, E.M. Gartner, G.P. Denbeaux, A soft X-ray microscope investigation into the effects of calcium chloride on tricalcium silicate hydration, Cement Concr. Res. 35 (1) (2005) 19–25, https://doi.org/10.1016/j.cemconres.2004.05.016.
[36] M.V. Petlovanyi, S.A. Zubko, V.V. Popovych, K.S. Sai, Physicochemical mechanism of structure formation and strengthening in the backfill massif when filling underground cavities, Voprosy Khimii i Khimicheskoi Tekhnologii 6 (2020) 142–150, https://doi.org/10.32434/0321-4095-2020-133-6-142-150.
[37] V.R.S. De Silva, P.G. Ranjith, M.S.A. Perera, B. Wu, T.D. Rathnaweera, The influence of admixtures on the hydration process of soundless cracking demolition agents(SCDA) for fragmentation of saturated deep geological reservoir rock formations, Rock Mech. Rock Eng. 52 (2019) 435–454, https://doi.org/10.1007/s00603-018-1596-9.
[38] N. Maneenoi, R. Bissen, S. Chawchai, Influence of admixtures on the performance of soundless chemical demolition agents and implications for their utilization, J. Sustain. Min. 21 (2) (2022) 3, https://doi.org/10.46873/2300-3960.1350.
[39] C. Gomez, T. Mura, Stresses caused by expansive cement in borehole, J. Eng. Mech. 110 (6) (1984) 1001–1005, 10.1061/(ASCE)0733-9399(1984)110:6(1001).
[40] Z.Z. Jin, H. Liao, W. Zhu, Splitting mechanism of rock and concrete under expansive pressure, in: Demolition and Reuse of Concrete and Masonry, Chemical Rubber Company Press, Abingdon, UK, 1988 141.
[41] T. Harada, T. Idemitsu, A. Watanabe, S.I. Takayama, The design method for the demolition of concrete with expansive demolition agents, in: Fracture Concrete and Rock, Springer, Berlin, Germany, 1989, 47–57.
[42] J.A. Gambatese, Controlled concrete demolition using expansive cracking agents, J. Construct. Eng. Manag. 129 (2003) 98–104, https://doi.org/10.1061/(ASCE)0733-9364(2003)129:1(98).
[43] T. Guo, S. Zhang, H. Ge, X. Wang, X. Lei, B. Xiao, A new method for evaluation of fracture network formation capacity of rock, Fuel 140 (2015) 778–787, https://doi.org/10.1016/j.fuel.2014.10.017.
[44] K.M. Habib, S. Shnorhokian, H. Mitri, Evaluating the application of rock breakage without explosives in undergroundconstruction—a critical review of chemical demolition agents, Minerals 12 (2022) 220, https://doi.org/10.3390/min12020220.
[45] H. Wiggenhauser, C. Kopp, J. Timofeev, H. Azari, Controlled cracks in concrete for non-destructive testing, J. Nondestr. Eval. 37 (2018) 67, https://doi.org/10.1007/s10921-018-0517-x.
[46] V. Saltas, D. Peraki, F. Vallianatos, The use of acoustic emissions technique in the monitoring of fracturing in concrete usingsoundless chemical demolition agent, Frat. Integrita Strutt. 13 (2019) 505–516, https://doi.org/10.3221/IGF-ESIS.50.42.
[47] Z. Zhong, P. Tao, H. Jin, L. Rong, Y. Cui, J. Liu A, Quantitative investigation on the fragmentation performance of SCDA in cracking steel fiber reinforced concrete, Construct. Build. Mater. 403 (1) (2023) 133133, https://doi.org/10.1016/j.conbuildmat.2023.133133.
[48] M. Hanif, M.-N.N.H. Al-Maghrabi, Effective use of expansive cement for the deformation and fracturing of granite, Gazi Univ. J. Sci. 20 (2007) 1–5.
[49] G.S.B. Bhardwaj, S. Sharma, Granite extraction and treatment techniques: a study on cost effective geo-technical aspects, Min. Eng. J. 11 (2010) 11–19.
[50] F.F.K. Tiam, R. Danwe, N. Konai, L. Meva'a, Experimental study and numerical simulation using extended finite ElementMethod (XFEM) combined with cohesive zone model (CZM), of crack growth induced by non-explosive expansive materials on two neighboring circular holes of A gneiss rock, Open J. Appl. Sci. 10 (2020) 592–612, https://doi.org/10.4236/ojapps.2020.1010042.
[51] V.R.S. De Silva, P.G. Ranjith, M.S.A. Perera, B. Wu, Artificial fracture stimulation of rock subjected to large IsotropicConfining stresses in saline environments: application in deep-sea gas hydrate recovery, Nat. Resour. Res. 28 (2019) 563–583, https://doi.org/10.1007/s11053-018-9409-0.
[52] V.R.S. De Silva, P.G. Ranjith, M.S.A. Perera, B. Wu, The effect of saturation conditions on fracture performance of differentsoundless cracking demolition agents (SCDAs) in geological reservoir rock formations, J. Nat. Gas Sci. Eng. 62 (2019) 157–170, https://doi.org/10.1016/j.jngse.2018.11.013.
[53] Y. Wang, X. Li, R.Q. Zhou, C.A. Tang, Numerical evaluation of the shear stimulation effect in naturally fractured formations, Sci. China Earth Sci. 59 (2) (2016) 371–383, https://doi.org/10.1007/s11430-015-5204-5.
[54] Z. Zhong, H. Zhang, X. Yang, R. Lou, B. Liu, Y. Chi, Y. Chen, A study on the optimal use of soundless cracking demolition agents in fragmentations of concrete based on the extended finite element method, Struct. Concr. 2022 (2022) 1–16, https://doi.org/10.1002/suco.202100902.
[55] W. Tang, C. Zhai, J. Xu, Y. Sun, Y. Cong, Y. Zheng, The influence of borehole arrangement of soundless cracking demolition agents (SCDAs) on weakening the hard rock, Int. J. Min. Sci. Technol. 31 (2021) 197–207, https://doi.org/10.1016/j.ijmst.2021.01.005.
[56] F. Ferry, K. Tiam, R. Danwe, N. Konaï, L. Meva'a, Experimental study and numerical simulation using extended finite element method (XFEM) combined with cohesive zone model (CZM), of crack growth induced by non-explosive expansive material on two neighboring circular holes of A gneiss rock, Open J. Appl. Sci. 10 (10) (2020), https://doi.org/10.4236/ojapps.2020.1010042.